EPJ Web of Conferences **158**, 01005 (2017) DOI: 10.1051/epjconf/201715801005
QFTHEP 2017

Charmless Hadronic Beauty Decays at LHCb

Timothy Williams,[1]⋆ on behalf of the LHCb collaboration

[1] *School of Physics and Astronomy, University of Birmingham, Birmingham, B15 2TT, United Kingdom*

Abstract. A summary of six LHCb results on the topic of charmless hadronic b-hadron decays is presented. These are comprised of: a search for the decay $B^0_s \to K^0_S K^+ K^-$ and updated branching fraction measurements of $B^0_{(s)} \to K^0_S h^+ h'^-$ decays (h=K,π) [1]; the first observation of the decays $B^0 \to p\overline{p}\pi^+\pi^-$, $B^0_s \to p\overline{p}K^+K^-$,$B^0_s \to p\overline{p}K^+\pi^-$ and strong evidence for the decay $B^0 \to p\overline{p}K^+K^-$ [2]; the first observation of the decay $B^0_s \to p\overline{\Lambda}K^-$ [3]; a search for the decay $B^0_s \to \phi\eta'$ [4]; the first observation of the decay $\Xi^-_b \to pK^-K^-$ [5] and evidence for CP-violation in $\Lambda^0_b \to p\pi^-\pi^+\pi^-$ decays [6].

1 Introduction

Charmless b-hadron decays provide fertile ground for studying CP violation and searching for the effects of new physics. These decays can typically proceed via either $b \to u$ tree level diagrams or $b \to s, d$ gluonic loop level diagrams. The former of these transisitons is heavily suppressed by the CKM matrix element V_{ub}, which means the tree and loop level diagrams often have similar amplitudes. The consequences of this are two fold; firstly the rates of these processes are sensitive to the presence of new physics entering into the loop diagrams and secondly CP-violation can arise from the interference of the tree and loop level diagrams. Therefore, by measuring branching fractions and *CP*-violation observables indirect searches for physics beyond the standard model can be performed. Furthermore, these measurements provide vital input for QCD calculations.

An overview of recent results from the LHCb experiment on the topic of charmless b- hadron decays is presented. These all make use of the Run I dataset collected by the LHCb detector during the years 2011 and 2012 which correspond to integrated luminosities of approximately $1\,\text{fb}^{-1}$ and $2\,\text{fb}^{-1}$ respectively. The LHCb detector is a single-arm forward spectrometer with a pseudorapidity coverage of $2 < \eta < 5$, which has an acceptance for $b\overline{b}$ pairs of $\sim 25\%$. The detector is specialised for studying particles containing beauty and charm quarks. The unique sub-detectors relevant for the studies presented here are: the silicon strip vertex locator (VELO) surrounding the beam pipe which gives an impact parameter resolution of $(15 \pm \frac{29}{p_T})$ μm [7] and the two ring imaging cherenkov sub-detectors (RICH) which provide excellent particle identification ability [8].

2 Updated Branching Fraction Measurements of $B^0_{(s)} \to K^0_S h^+ h'^-$ Decays

Several extensions to the standard model, which involve the presence of new particles, introduce additional weak phases to the amplitude of $b \to q\bar{q}s$ (q=s,d,u) decays [9]. As these new physics effects

⋆e-mail: timothy.williams@cern.ch

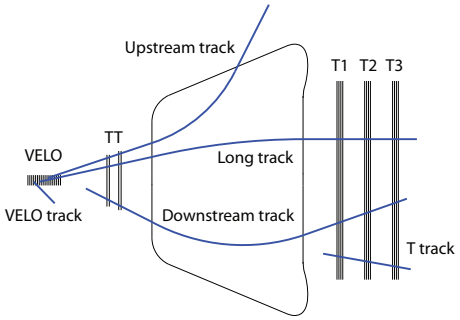

Figure 1. The different track types at LHCb. K^0_S particles that decay inside the VELO produce Long tracks and K^0_S particles that decay outside the VELO produce downstream tracks [12].

only enter via the loop diagrams which dominate the amplitudes of these charmless decays, the overall weak phase of $b \to c\bar{c}s$ decays would remain unchanged. Therefore, deviations in the values of weak phase measurements between those determined from $b \to q\bar{q}s$ (q=s,d,u) decays and from $b \to c\bar{c}s$ decays could be an indication of new physics. Mixing induced CP violation has been measured in charmed decays through channels such as $B^0 \to J/\psi K^0_S$ [10], and a time-dependent flavour tagged analysis of the three body Dalitz plot for $B^0 \to K^0_S\pi^+\pi^-$ and $B^0 \to K^0_S K^+K^-$ decays would facilitate a comparison with charmless decays.

Unfortunately, the size of the data samples currently available at LHCb mean a flavour tagged time-dependent analysis of these decay modes is not feasible. In fact, the $B^0_s \to K^0_S K^+K^-$ is still unobserved. Therefore, the first aim is to observe all decay modes and develop selections that can later be used for Dalitz analyses. Previous LHCb results on these channels, making use of 1 fb^{-1} of 7 TeV data collected in 2011, made the first observation of the decay modes $B^0_s \to K^0_S\pi^+\pi^-$, $B^0_s \to K^0_S K^\pm\pi^\mp$ and measured the branching fraction of all observed $B^0_{(s)} \to K^0_S h^+h'^-$ decays relative to the well measured channel $B^0 \to K^0_S\pi^+\pi^-$ [11]. Updated branching fraction results, which now include the 2 fb^{-1} of 8 TeV data collected in 2012, are presented below along with an updated search for the decay $B^0_s \to K^0_S K^+K^-$.

Due to the long lived nature of the neutral K^0_S particle, two separate reconstruction categories are used in this measurement. If the K^0_S decays inside the LHCb VELO the tracks from the daughter particles can be fully reconstructed. However, if the K^0_S decays outside of the VELO there is less precise tracking information available and the mass resolution of the reconstructed K^0_S is broader. Consequently, separate mass fits are required for each reconstruction category. As depicted in Figure 1, when the K^0_S decays outside of the VELO it is labelled a downstream event and when the K^0_S decays inside the VELO it is labelled as a long event.

A BDT classifier is used to separate signal and background events. The variables that enter into this classifier are deliberately chosen to avoid significant variations in efficiency over the phase space of the decay as such variations would be undesirable for future three body Dalitz plot analyses. There are two separate optimisations of the requirement on the BDT output for each final state; one for the favoured mode and one for the suppressed mode. It is possible for decays such as $\Lambda^0_b \to K^0_S p\pi^-$ to remain present as mis-ID backgrounds, therefore particle identification requirements are imposed to

Decay	Downstream Yield	Long Yield	Branching Fraction
$B^0 \to K^0_S \pi^+\pi^-$	2766 ± 66	1411 ± 45	
$B^0 \to K^0_S K^\pm \pi^\mp$	261 ± 24	160 ± 17	$(6.1 \pm 0.5 \pm 0.7 \pm 0.3) \times 10^{-6}$
$B^0 \to K^0_S K^+ K^-$	1133 ± 39	685 ± 29	$(27.2 \pm 0.9 \pm 01.6 \pm 1.1) \times 10^{-6}$
$B^0_s \to K^0_S \pi^+\pi^-$	146 ± 19	74 ± 11	$(9.5 \pm 1.3 \pm 1.5 \pm 0.4) \times 10^{-6}$
$B^0_s \to K^0_S K^\pm \pi^\mp$	1100 ± 41	568 ± 28	$(84.3 \pm 3.5 \pm 7.4 \pm 3.4) \times 10^{-6}$
$B^0_s \to K^0_S K^+ K^-$	12 ± 6	7 ± 4	$\in [0.4 - 2.5] \times 10^{-6}$ at 90% C.L.

Table 1. Signal yield and branching fraction results for each of the $B^0_{(s)} \to K^0_S h^+ h'^-$ decay modes

remove such backgrounds. There can be further backgrounds from B and Λ^0_b decays where the decay has proceeded through an intermediate charm (charmonium) resonance, for example $B^0 \to \bar{D} K^0_S$. These backgrounds are removed with explicit mass vetos of width 30(48) MeV around the world average mass of the charm (charmonium) resonance.

In order to extract the signal yields, the selected data samples are separated into 12 mutually exclusive categories; three separate final states, two different opitmisations and two different reconstruction categories. An unbinned simultaneous extended maximum likelihood fit to all categories is then performed. The signal decays are modelled with the sum of two Crystal Ball functions (CB) [13] and combinatorial background is modelled with a linear function. Cross-feed backgrounds, where events from one signal final state are mis-identified as another, are modelled with emperical shapes taken from simulated samples and Gaussian constraints are applied to the relative yield of these backgrounds. Partially reconstructed backgrounds from decays such as $B^0_s \to (K^{*0} \to K^0_S \pi^0)(\bar{K}^{*0} \to K^- \pi^+)$ are modelled with ARGUS functions [14]. The results of this fit for the favoured and suppressed optimisations are shown in Figure 2 and Figure 3 respectively. The resulting signal yields are shown in Table 1.

After correcting efficiencies for the variation over the phase space of the decay, the ratio of branching fractions (relative to the decay $B^0 \to K^0_S \pi^+\pi^-$) is determined separately for each reconstruction category. These are then combined for each decay mode by performing a minimum χ^2 fit where the convariance matrix includes the statistical and systematic uncertainties. The world average branching fraction measurement, with the previous LHCb result omitted, for the $B^0 \to K^0_S \pi^+\pi^-$ mode is then used to obtain the branching fraction results shown in Table 1.

The significance of the observed signal yield for the $B^0_s \to K^0_S K^+ K^-$ mode is equivalent to 2.5 Gaussian standard deviations; this decay mode still remains unobserved. Therefore, a 90% confidence level interval is instead derived using the Feldman-Cousins method [15].

Despite not observing the $B^0_s \to K^0_S K^+ K^-$ mode, these branching fraction measurements offer improved precision over, whilst still being consistent with, the previous LHCb results [11]. Work is now underway to perform Daltiz plot analyses of the dominant decay modes - $B^0 \to K^0_S \pi^+\pi^-$, $B^0_s \to K^0_S K^\pm \pi^\mp$ and $B^0 \to K^0_S K^+ K^-$.

3 First Observation of the Decay $B^0_s \to p\bar{\Lambda} K^-$

The inclusive branching fraction of B decays to baryonic final states is $\sim 7\%$ of the total decay width; many experimental studies of baryonic B decays have been carried out. At previous e^+e^- collider experiments the observation of many baryonic decays of B^0 and B^+ mesons have been reported [16, 17]. More recently, the first observation of a baryonic B^+_c decay was reported by the LHCb collaboration [18]. However, the baryonic decay of a B^0_s meson has never previously been observed. The only

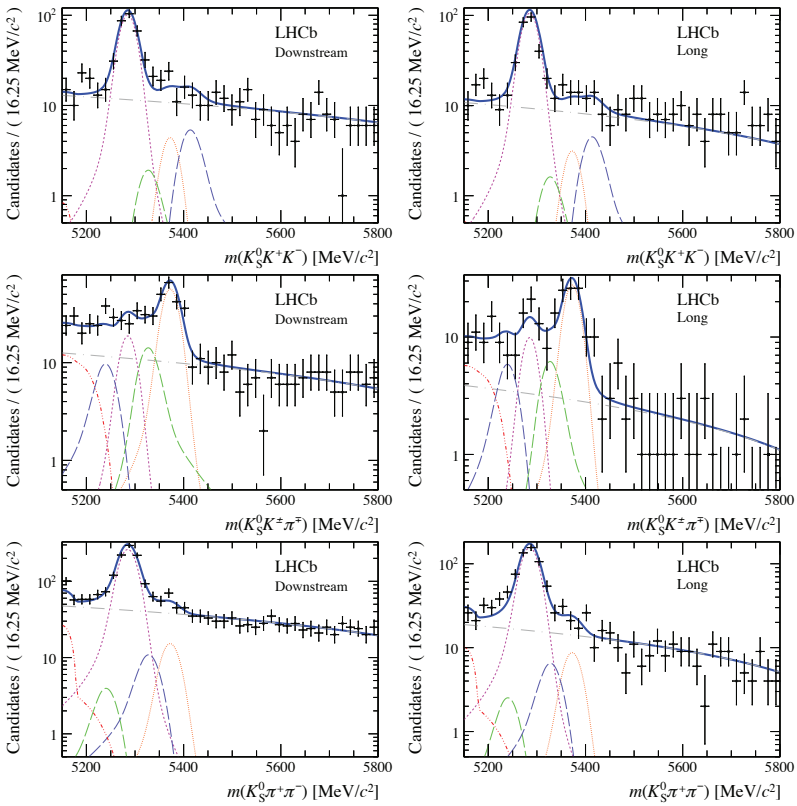

Figure 2. Invariant mass distributions for each possible final state with the favoured mode selection. The Downstream(Long) reconstruction category is shown on the right(left). The B^0 (B^0_s) signal candidates are shown by the magenta (orange) short dashed line, partially reconstructed backgrounds are shown by the red double dot dash line, the combinatorial background is shown by the grey dot dash line and the blue and green long dashed lines are mis-ID backgrounds. The full fit is shown by the solid blue line. [1]

evidence for such a decay is reported by the Belle collaboration, where 4.4σ evidence for the decay $B^0_s \to \overline{\Lambda}_c^- \Lambda \pi^+$ was seen [19].

One interesting aspect of baryonic B decays is the hierachy of branching fractions; multi-body baryonic B decays generally have higher branching fractions than two body baryonic decays. It is predicted that the decay $B^0_s \to p\overline{\Lambda}K^-$ has a branching fraction of the order of 10^{-6} which, based on similar charmless b decays, suggests it is likely to be accessible with the LHCb Run I dataset [20, 21]. It is also predicted that CP violating asymmetries in the decay $B^0 \to p\overline{\Lambda}\pi^-$ could be as high as $\sim 12\%$ [22], which provides extra motivation for studying the $B^0_{(s)} \to p\Lambda h$ family of decays. For these reasons, a search for the decay $B^0_s \to p\overline{\Lambda}K^-$ has been performed using the LHCb Run I dataset.

The branching fraction of the $B^0_s \to p\overline{\Lambda}K^-$ is measured relative to the topologically very similar decay $B^0 \to p\overline{\Lambda}\pi^-$ in order to reduce systematic uncertainties. The branching fraction of this decay, $\mathcal{B}(B^0 \to p\overline{\Lambda}\pi^-) = (3.14 \pm 0.29) \times 10^{-6}$, has been previously measured by the BaBar and Belle collaborations [23]. For the same reasons as described in Section 2, the data is separated into two reconstruction categories, depending on whether the $\overline{\Lambda}$ is reoncstructed inside or outside of the LHCb

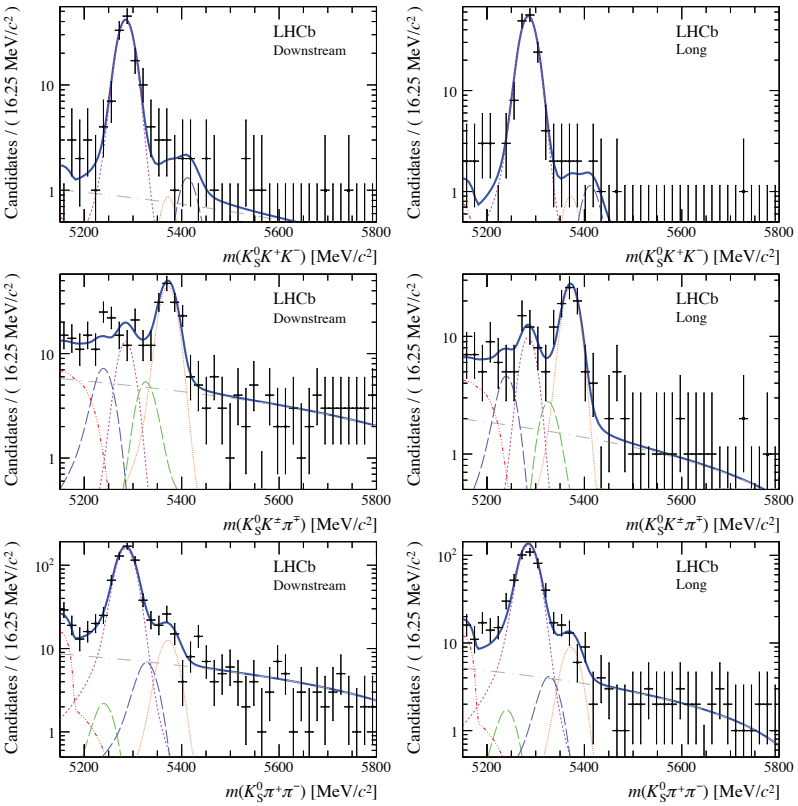

Figure 3. Invariant mass distributions for each possible final state with the suppressed mode selection. The Downstream(Long) reconstruction category is shown on the right(left). The individual fit components follow the same convention as Figure 2. [1]

VELO. After applying explicit mass vetoes to remove background events from the decay $B^0 \to \overline{\Lambda}_c^- p$, an MLP classifier is used to reduce combinatorial background. There are then further PID requirements applied to the p and K^-/π^- from the B meson, but no PID requirements are placed on the p from the $\overline{\Lambda}$ because no evidence for contamination from $K^0_S \to \pi^+\pi^-$ decays has been found.

The signal and control channel yields are extracted by performing an extended maximum likelihood fit to the signal and control channel simultaneously. The results of these fits for both years of data taking and both reconstruction categories are shown in Figure 4. These mass fit models include components for: signal, combinatorial background and partially reconstructed background from the decays $B^0 \to p\overline{\Sigma}\pi^-$ and $B^0_s \to p\overline{\Sigma}K^-$.

It is clear from Figure 4 that signal events are unambiguously present in both channels; the resulting total yields are $N(B^0_s \to p\overline{\Lambda}K^-) = 234 \pm 29$ and $N(B^0 \to p\overline{\Lambda}\pi^-) = 519 \pm 28$. This is the first observation of a baryonic B^0_s decay, with a statistical significance of greater than 15 gaussian standard deviations. The branching fraction is subsequently measured to be,

$$\mathcal{B}(B^0_s \to p\overline{\Lambda}K^-) + \mathcal{B}(\bar{B}^0_s \to p\overline{\Lambda}K^-) = \left[5.46 \pm 0.61 \pm 0.57 \pm 0.50(\mathcal{B}) \pm 0.32(\frac{f_s}{f_d})\right] \times 10^{-6}$$

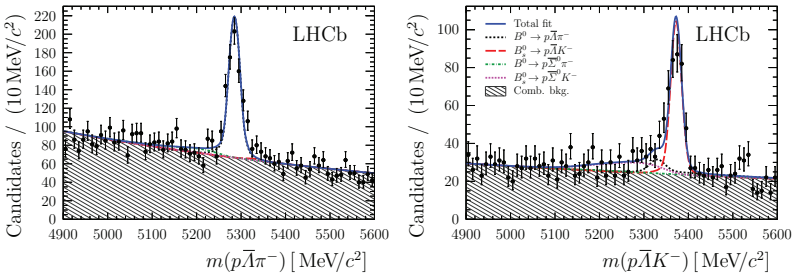

Figure 4. Left (Right): The invariant mass distribution of $B^0 \to p\overline{\Lambda}\pi^-$ ($B_s^0 \to p\overline{\Lambda}K^-$) channel candidate events. The grey shaded area is combinatorial background, partially reconstructed backgrounds are represented by the dot and dot dash green and pink lines and signal is represented by black and red dashed lines. The full fit is shown by the solid blue line. [3]

where the first uncertainty is statistical, the second uncertainty is systematic, the third is due to the control channel branching fraction and the fourth is due to the knowledge of the ratio of B_s^0/B^0 b quark fragmentation fractions ($\frac{f_s}{f_d}$). The sum of the branching fractions from both B_s^0 and $\overline{B}_s^0$ is quoted because the identical final states mean it is not possible to determine the flavour of the B_s^0 meson without a flavour tagged analysis.

Another area of interest in the study of baryonic B decays is threshold enhancement in the baryon anti-baryon system. This effect has previously been observed by the BaBar and Belle collaborations in several baryonic B decays [17]. This effect is investigated in the $B^0 \to p\overline{\Lambda}\pi^-$ and $B_s^0 \to p\overline{\Lambda}K^-$ decays by using the *sPlot* technique to perform a background subtraction and correct for efficiency variations across the phase space of the decay [24]. The efficiency corrected and background subtracted invariant mass distributions for the $p\ \overline{\Lambda}$ system are shown in Figure 5; clear threshold enhancement is observed.

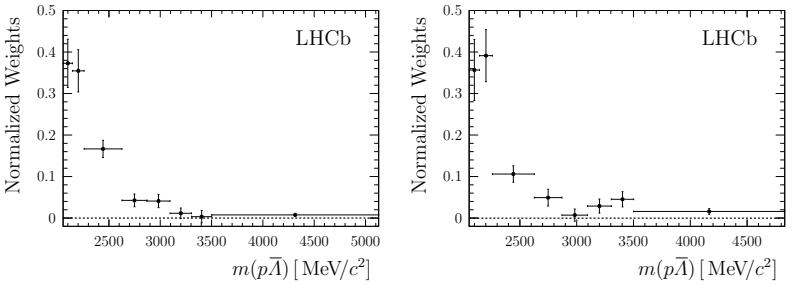

Figure 5. Left (Right): Normalised, background subtracted and efficiency corrected m($p\ \overline{\Lambda}$) invariant mass distributions for the $B^0 \to p\overline{\Lambda}\pi^-$ ($B_s^0 \to p\overline{\Lambda}K^-$) candidates. [3]

4 Search for $B^0_{(s)} \to p\overline{p}h^+h^-$ decays

As described in Section 3 the baryonic decay of a B_s^0 meson has now been observed. However, a four body baryonic decay of the B_s^0 meson is still to be observed and previous results for the B^0 meson only

set an upper limit $\mathcal{B}(B^0 \to p\bar{p}\pi^+\pi^-) < 2.5 \times 10^{-4}$ at 90% confidence level[25]. There is additional motivation in studying four body baryonic B meson decays because they are an ideal place to search for CP violation using triple-product correlations (TPCs); in contrast to the case of three body decays, they do not involve the spins of the final state particles. This motivation is strengthened by the first evidence of CP violation in baryonic B decays being seen in $B^+ \to p\bar{p}K^+$ decays [26] and predictions of CP violation as high as 20% in other baryonic B decays [27].

A search for the family of decays $B^0_{(s)} \to p\bar{p}h^+h^-$ is reported, where h is a kaon or pion. The branching fractions of these decays are measured relative to the decay $B^0 \to J/\psi K^{*0}$, where the resonances are reconstructed through the $J/\psi \to p\bar{p}$ and $K^{*0} \to K^+\pi^-$ decay channels. In order to remove charm and charmonium resonances in the signal channels the requirement $m(p\bar{p}) < 2.85\,\text{GeV}$ is imposed on the signal channels and specfic mass vetoes are applied to remove Λ_c^+ and D^0 decays. The selection further consists of a BDT, which makes use of 15 variables, to reduce combinatorial background and PID requirements remove mis-ID backgrounds.

The signal yields are extracted with an extended maximum likelihood fit which is simultaneous across the invariant masses of all 3 possible final states: $m(p\bar{p}K^+\pi^-)$, $m(p\bar{p}K^+K^-)$ and $m(p\bar{p}\pi^+\pi^-)$. A separate fit is performed for the $B^0 \to J/\psi K^{*0}$ control channel which is multi-dimensional for the $m(p\bar{p}K^+\pi^-)$, $m(p\bar{p})$ and $m(K^+\pi^-)$ invariant masses. These fits are shown in Figure 6 and the resulting yields and branching fractions are shown in Table 2. This is the first observation of the decays $B^0 \to p\bar{p}\pi^+\pi^-$ and $B^0_s \to p\bar{p}K^+K^-$ with significances of $> 25\sigma$. The decay $B^0_s \to p\bar{p}K^+\pi^-$ is also observed with a significance of 6.5σ, there is strong evidence for the decay $B^0 \to p\bar{p}K^+K^-$ at the level of 4.1σ and evidence at the level of 2.6σ is seen for the $B^0_s \to p\bar{p}\pi^+\pi^-$ decay. A limit is set on the $B^0_s \to p\bar{p}\pi^+\pi^-$ channel by integrating the likelihood with a uniform prior in the region of positive branching fraction.

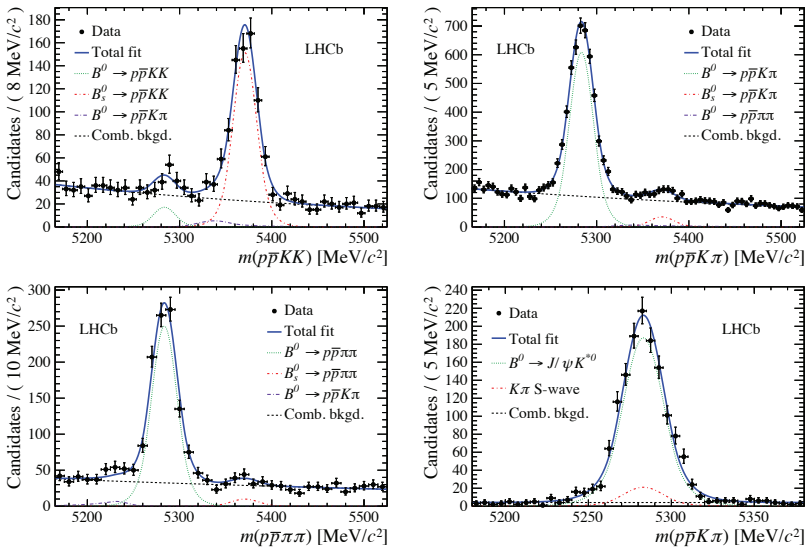

Figure 6. Top Left, Top Right and Bottom Left: Signal channel simultaneous mass fit to all three final states. B^0 signal is shown by the dotted green line, B^0_s signal by the dot dash red line and cross feed background is shown by the dot dash purple line. Bottom Right: Projection of the 3D control channel mass fit. [2]

Channel	Yield	Branching Fraction/10^{-6}
$B^0 \to p\overline{p}K^+K^-$	68 ± 17	0.113 ± 0.028 ± 0.011 ± 0.008
$B^0 \to p\overline{p}K^+\pi^-$	4155 ± 83	5.9 ± 0.3 ± 0.3 ± 0.4
$B^0 \to p\overline{p}\pi^+\pi^-$	902 ± 35	2.7 ± 0.1 ± 0.1 ± 0.2
$B^0_s \to p\overline{p}K^+K^-$	635 ± 32	4.2 ± 0.3 ± 0.2 ± 0.3 ± 0.3
$B^0_s \to p\overline{p}K^+\pi^-$	246 ± 39	1.3 ± 0.21 ± 0.11 ± 0.09 ± 0.08
$B^0_s \to p\overline{p}\pi^+\pi^-$	39 ± 16	< 0.66 at 90% CL

Table 2. Signal yields and branching fraction results for the six $B^0_{(s)} \to p\overline{p}h^+h^-$ decays. The first uncertainty is statistical, the second systematic, the third is due to the uncertainty on the normalisation channel branching fraction and the fourth (in the case of B^0_s mesons) is due to the ratio of B^0_s/B^0 fragmentation fractions.

As described in Section 3, threshold enhancement has been observed in the baryon antibaryon system of several B meson decays. To investigate threshold enhancement in the $B^0 \to p\overline{p}K^+\pi^-$ decay, the *sPlot* technique is again used to perform a background subtraction and correct for the efficiency variation across the phase space of the decay. The normalised, background subtracted and efficiency corrected distribution of $m(p\overline{p})$ can be seen in Figure 7 [24]. As with the decay $B^0_s \to p\overline{\Lambda}K^-$ (see Figure 5), clear threshold enhancement is present.

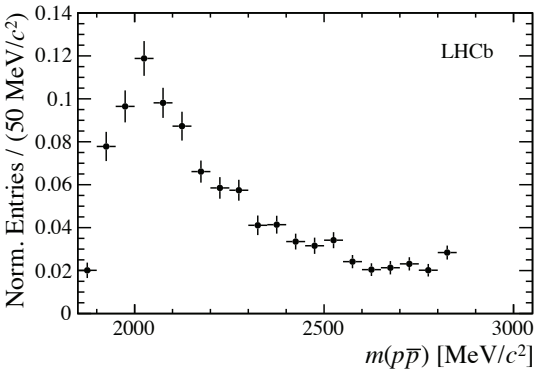

Figure 7. Normalised, background subtracted and efficiency corrected $m(p\overline{p})$ distribution for the $B^0 \to p\overline{p}K^+\pi^-$ decay channel. [2]

5 Search for the decay $B^0_s \to \eta'\phi$

Current experimental knowledge of B^0_s decays to a light pseudoscalar (P) meson and a vector meson (V) is very limited and theoretical predictions for the branching fractions of such decays have large uncertainties and cover a large range. For example, a QCD factorisation approach can yield the result $\mathcal{B}(B^0_s \to \eta'\phi) = (0.05^{1.18}_{-0.19}) \times 10^{-6}$ [28], whereas a perturbative QCD approach yields the prediction $\mathcal{B}(B^0_s \to \eta'\phi) = (20.0^{+16.3}_{-9.1}) \times 10^{-6}$ [29] (see Table 1 in Ref. [4] for a summary of theoretical predictions). These large uncertainties are a consequence of the currently limited knowledge of penguin contributions, the ω- ϕ mixing angle, the s-quark mass and form factors. Therefore, a measurement of $\mathcal{B}(B^0_s \to \eta'\phi)$ would be a useful input to the knowledge of B^0_s to ϕ form factors and would subsequently improve the accuracy of branching fraction predictions for $B^0_s \to P\phi$ decays.

A search for the decay $B_s^0 \to \eta'\phi$ is reported, where the η' is reconstructed through the channel $\eta' \to \pi^+\pi^-\gamma$ and the ϕ through the channel $\phi \to K^+K^-$. The well studied decay $B^+ \to K^+\eta'$ is used as a control channel due to its relatively large branching fraction $\mathcal{B}(B^+ \to K^+\eta') = (70.6 \pm 2.5) \times 10^{-6}$ and the presence of only combinatorial background [23, 30]. The selection makes use of a BDT with 9 variables to reject the majority of combinatorial background and particle identification requirements are imposed on the hadrons and the photon from the η'.

The signal yields are extracted with an extended maximum likelihood fit to the $B_s^0 \to \eta'\phi$ and $B^+ \to K^+\eta'$ channels simultaneously. The PDF used in the $B_s^0 \to \eta'\phi$ ($B^+ \to K^+\eta'$) channel is two dimensional for the $m(\eta'\phi)$ and $m(\pi^+\pi^-\gamma)$ ($m(\eta' K^+)$ and $m(\pi^+\pi^-\gamma)$) variables. In the case of the $B_s^0 \to \eta'\phi$ channel, there is an irreducible background from $B_s^0 \to \phi\phi$ decays where one of the ϕ mesons decays through $\phi \to K^+K^-$ and the other through $\phi \to \pi^+\pi^-\pi^0$ but one of the photons from the decay of the π^0 is not reconstructed. This background is therefore modelled in the fit with a two-dimensional Gaussian kernel function [31]. The fit results for the $B_s^0 \to \eta'\phi$ channel are shown in Figure 8.

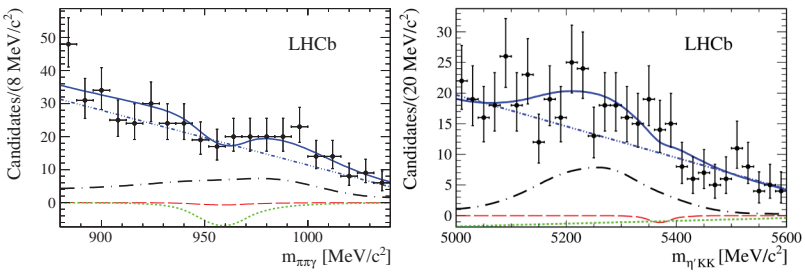

Figure 8. Left (Right): Distributions of m($\pi^+\,\pi^-\,\gamma$) (m($\eta'\,\phi$)) for the $B_s^0 \to \eta'\phi$ channel. The solid blue line represents the result of the two-dimensional simultaneous fit to both channels. The red dashed line shows the signal component, the green dashed line shows the combinatorial background with a real η', the blue dot-dash line shows combinatorial background without a real η' and the black dot-dash line is the irreducible $B_s^0 \to \phi\phi$ background described in the text. [4]

The yields from this fit are $N(B_s^0 \to \eta'\phi) = -3.2^{+5.0}_{-3.8}$ and $N(B^+ \to K^+\eta') = 11081 \pm 127$, therefore bayesian upper limits are set on $\mathcal{B}(B_s^0 \to \eta'\phi)$ using a uniform prior. The resulting limit is,

$$\mathcal{B}(B_s^0 \to \eta'\phi) < 0.82(1.01) \times 10^{-6} \text{ at } 90\% \ (95\%) \text{ CL},$$

which is the first upper limit to be set on $\mathcal{B}(B_s^0 \to \eta'\phi)$. This result is consistent with the lower end of the range of predictions available for this branching fraction; the central values of several predictions are inconsistent with this result, see for example Refs. [29, 32–34]. This result therefore provides very useful constraints on the theoretical models used to predict branching fractions and CP asymmetries of charmless B_s^0 decays to a pseudoscalar and vector meson final state.

6 Search for the decays $\Xi_b^-, \Omega_b^- \to ph^-h'^-$

Prior to the collection of the Run I dataset by LHCb, opportunities to study charmless decays of b-baryons were very limited. Consequently, the only observed decays were $\Lambda_b^0 \to p\pi^-$ and $\Lambda_b^0 \to pK^-$ by the CDF collaboration [35]. More recently, LHCb has observed the Λ_b^0 decays $\Lambda_b^0 \to pK_s^0\pi^-$ [36], $\Lambda_b^0 \to \Lambda\pi^+\pi^-$, $\Lambda_b^0 \to \Lambda K^+\pi^-$, $\Lambda_b^0 \to \Lambda K^+K^-$ [37] and $\Lambda_b^0 \to \Lambda\phi$ [38]. There has also been evidence at the level of 3σ seen for the decay $\Lambda_b^0 \to \Lambda\eta$ [21]. However a charmless decay of a Ξ_b^- or Ω_b^- baryon is

yet to be observed, therefore a search for the decays $\Xi_b^-, \Omega_b^- \to ph^-h'^-$ where h=K^-, π^- is presented. It is not currently possible to measure the absolute branching fractions of Ξ_b^- and Ω_b^- decays because the fragmentation fractions, $f_{\Xi_b^-}$ and $f_{\Omega_b^-}$, are not known. This search uses the topologically similar and well measured decay $B^- \to K^+K^-K^-$ as a control channel, therefore the reported results are the product of branching fraction and ratio of fragmentation fractions, denoted $R_{ph^-h'^-}$.

The event selection firstly consists of a neural network, which makes use of 8 variables, to reduce combinatorial background. A tight particle identification requirement is then imposed on the proton to reject background from $B^- \to K^+h^-h'^-$ decays. Further particle identification requirements on the other hadrons are optimised in a manner that ensures mutually exclusive samples for each possible final state. There are then vetoes applied to remove charm backgrounds from decays such as $\Xi_b^- \to \Xi_c^0 h^- \to pK^-h^-$ and $B^- \to D^0K^- \to K^+K^-K^-$.

The signal yields are extracted using an extended unbinned maximum likelihood fit which is simultaneous across the invariant mass distributions of the three possible final states ($m(pK^-K^-)$, $m(pK^-\pi^-)$ and $m(p\pi^-\pi^-)$). The use of a simultaneous fit allows cross-feed background, where candidates from one final state are mis-identified as another, to be constrained to expected values. The control channel yield is extracted with a separate fit to the $m(K^+K^-K^-)$ distribution. There are also partially reconstructed backgrounds present that have to be modelled in the fit. In the $m(ph^-h'^-)$ distributions these arise from decays such as $\Xi_b^- \to N^+h^-h'^- \to p\pi^0h^-h'^-$ where the π^0 is not reconstructed. These backgrounds are modelled with an ARGUS function [14] convolved with a Gaussian function.

The projections of the simultaneous fit and the separate control channel fit are shown in Figure 9; the fitted yields and subsequent branching fraction times fragmentation fraction ratios are shown in Table 3. The significance of the $\Xi_b^- \to pK^-K^-$ signal yield is 8.7σ; this is the first observation of a charmless Ξ_b^- decay. There is also 3.4σ evidence for the decay $\Xi_b^- \to pK^-\pi^-$, but all other signal yields have a significance of $< 2.0\sigma$ meaning the charmless decay of an Ω_b^- baryon still remains unobserved. For these channels with significance $< 2.0\sigma$ an upper limit is set on $R_{ph^-h'^-}$ by integrating the likelihood after multiplying by a prior probability distribution which is uniform in the positive region.

Although it is not possible to measure absolute branching fractions, the observation of the $\Xi_b^- \to pK^-K^-$ decay means it is possible to measure the relative branching fractions of the Ξ_b^- decays. This cancels the dependance on fragmentation fractions, which is useful for comparisons with theoretical predictions. The measured relative branching fractions are,

$$\frac{\mathcal{B}(\Xi_b^- \to pK^-\pi^-)}{\mathcal{B}(\Xi_b^- \to pK^-K^-)} = 0.98 \pm 0.27(stat) \pm 0.09(syst),$$

$$\frac{\mathcal{B}(\Xi_b^- \to p\pi^-\pi^-)}{\mathcal{B}(\Xi_b^- \to pK^-K^-)} = 0.28 \pm 0.16(stat) \pm 0.13(syst) < 0.56(0.63),$$

where the upper limit quoted is at the 90%(95%) CL.

It is of interest to study the intermediate resonances that occur in the $\Xi_b^- \to pK^-K^-$ channel; it is hoped that when larger data samples are available an amplitude analysis to dis-entangle the intermediate resonances and to search for CP violation can be performed. Whilst this is not currently possible, it is still of interest to inspect the intermediate resonances. Figure 10 shows the background subtracted and efficiency corrected $m(pK^-)_{min}$ distribution for the $\Xi_b^- \to pK^-K^-$ channel; $m(pK^-)_{min}$ is the smaller of the two possible $m(pK^-)$ values for each candidate. This distribution shows clear peaks consistent with the $\Lambda(1520)$ and a combination of the $\Lambda(1670)$ and $\Lambda(1690)$ states. The less prominent peaks at higher mass suggest the possibility of further states being present.

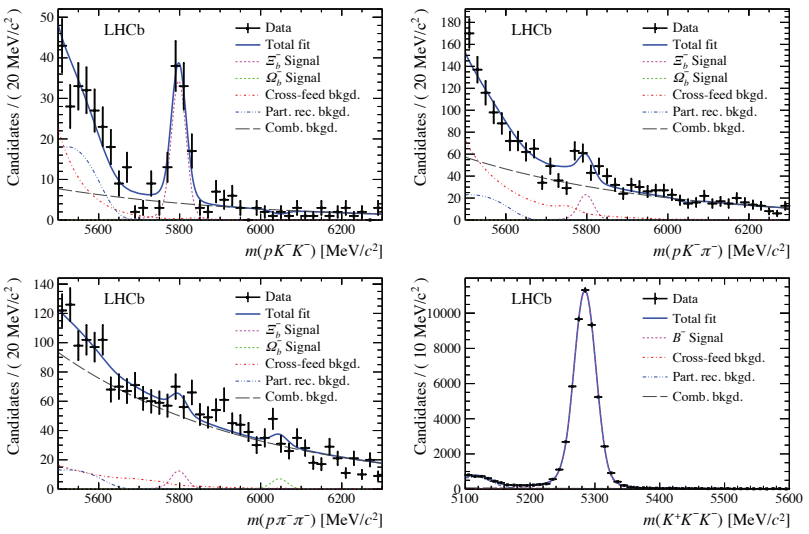

Figure 9. Top Left, Top Right and Bottom Left: Projections of the simultaneous fit to the $m(ph^-h'^-)$ final states. Bottom Right: The control channel fit to $m(K^+K^-K^-)$ mass distribution. The full fits are shown by the blue solid line, Ξ_b^- and B^- signal components are shown by the pink dashed line, Ω_b^- signal components are shown by the green dashed line, cross-feed backgrounds are shown by the red dot-dash line, partially reconstructed backgrounds are shown by the blue double dot-dash line and combinatorial background is shown by the grey long dashed line. [5]

Channel	Yield	$R_{ph^-h'^-}$ (10^{-5})
$\Xi_b^- \to pK^-K^-$	82.9 ± 10.4	$265 \pm 35 \pm 47$
$\Xi_b^- \to pK^-\pi^-$	59.6 ± 16.0	$259 \pm 64 \pm 49$
$\Xi_b^- \to p\pi^-\pi^-$	33.2 ± 17.9	$< 147(166)$
$\Omega_b^- \to pK^-K^-$	-2.8 ± 2.5	$< 18(22)$
$\Omega_b^- \to pK^-\pi^-$	-7.6 ± 9.2	$< 51(62)$
$\Omega_b^- \to p\pi^-\pi^-$	20.1 ± 13.8	$< 109(124)$
$B^- \to K^+K^-K^-$	50490 ± 250	

Table 3. Yield and $R_{ph^-h'^-}$ results for each of the decay channels studied, where $R_{ph^-h'^-}$ is the product of branching fraction and the ratio of Ξ_b^-/Ω_b^- and B^- fragmentation fractions $\frac{f_{\Xi_b^-/\Omega_b^-}}{f_{B^-}}$. The limits set are at the (90%)95% confidence level.

7 Search for CP violation in $\Lambda_b^0 \to p\pi^-\pi^+\pi^-$ decays

The levels of CP violation predicted by the standard model, through the CKM mechanism, are not enough to explain the matter-antimatter imbalance in the universe. It is therefore of great interest to search for additional sources of CP violation to explain the existence of a matter dominated universe. Thus far, CP violation has been observed in B_s^0 [39], B^+ [40] and B^0 [41] meson decays but has not been seen in the decay of a Λ_b^0 baryon. The LHC produces a copious amount of Λ_b^0 baryons; approximately 20% of all b hadrons prodcued are Λ_b^0 baryons. Therefore, LHCb exploits these unprecedented Λ_b^0 samples by searching for CP violation in $\Lambda_b^0 \to p\pi^-\pi^+\pi^-$ decays.

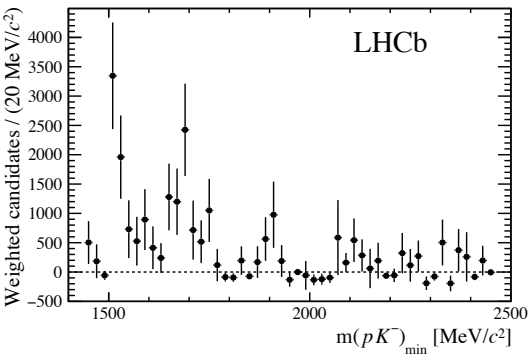

Figure 10. Background subtracted and efficiency corrected $m(pK^-)_{min}$ distribution for $\Xi_b^- \to pK^-K^-$ candidates. [5]

This search is performed by studying asymmetries in the $\hat{T}$ operator, which is the unitary operator that reverses both momentum and spin three-vectors [1]. Scalar triple products are defined,

$$C_{\hat{T}} = \vec{p}_p \cdot (\vec{p}_{\pi^-} \times \vec{p}_{\pi^+}), \qquad \bar{C}_{\hat{T}} = \vec{p}_p \cdot (\vec{p}_{\pi^+} \times \vec{p}_{\pi^-}) \tag{1}$$

where $\vec{p}_h$ is the momentum of the final state hadron, h, in the Λ_b^0 centre-of-mass frame. The π^- with the largest momenta in the Λ_b^0 rest frame is used (π^-_{fast}). Asymmetries can then be defined as,

$$A_{\hat{T}}(C_{\hat{T}}) = \frac{N(C_{\hat{T}} > 0) - N(C_{\hat{T}} < 0)}{N(C_{\hat{T}} > 0) + N(C_{\hat{T}} < 0)}, \qquad \bar{A}_{\hat{T}}(\bar{C}_{\hat{T}}) = \frac{\bar{N}(-\bar{C}_{\hat{T}} > 0) - \bar{N}(-\bar{C}_{\hat{T}} < 0)}{\bar{N}(-\bar{C}_{\hat{T}} > 0) + \bar{N}(-\bar{C}_{\hat{T}} < 0)} \tag{2}$$

where $N(\bar{N})$ is the number of Λ_b^0 ($\overline{\Lambda}_b^0$) decays satisfying the given condition. Using these asymmetries, CP violation and P violation observables are defined:

$$a_{CP}^{\hat{T}-odd} = \frac{1}{2}(A_{\hat{T}} - \bar{A}_{\hat{T}}), \qquad a_p^{\hat{T}-odd} = \frac{1}{2}(A_{\hat{T}} + \bar{A}_{\hat{T}}). \tag{3}$$

Any deviation from zero in these operators would indicate the presence of CP/P violation. The advantage of using triple product asymmetries is that they are largely insensitive to prodcution asymmetries and charge asymmetries caused by the LHCb detector.

The event selection makes use of a BDT to reduce combinatorial background and optimised particle identification requirements. An extended unbinned maximum likelihood fit to the $m(p\pi^-\pi^+\pi^-)$ invariant mass distribution is used to extract the total signal yield of both Λ_b^0 and $\overline{\Lambda}_b^0$ decays. This fit is shown in Figure 11 and has several components: signal decays are modelled by a Gaussian core with power law tails [13]; combinatorial background is modelled with an exponential function; partially reconstructed backgrounds from five body Λ_b^0 decays where one particle is not reconstructed are modelled with an ARGUS [14] function convolved with a Gaussian and mis-ID backgrounds are modelled with shapes fixed from simulation. The signal yield from this fit is $N(\Lambda_b^0 \to p\pi^-\pi^+\pi^-) = 6646 \pm 105$ and is the first observation of the decay $\Lambda_b^0 \to p\pi^-\pi^+\pi^-$.

In order to extract the CP and P observables in Eqn. (3), the data sample is split into four categories by Λ_b^0 or $\overline{\Lambda}_b^0$ flavour and sign of $C_{\hat{T}}$ or $\bar{C}_{\hat{T}}$. An extended unbinned maximum likelihood fit is then

[1]The $\hat{T}$ operator is different to the time-reversal operator

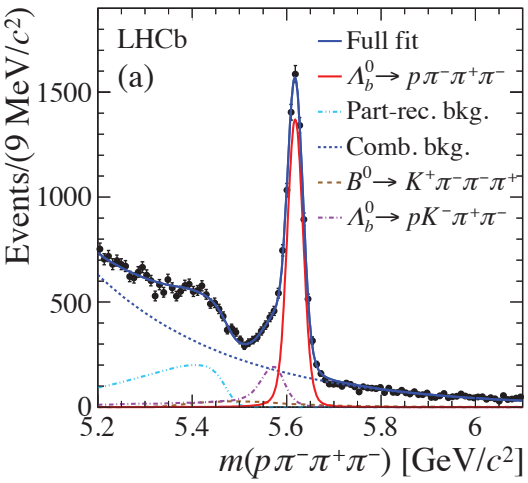

Figure 11. The invariant mass distribution of $\Lambda_b^0 \to p\pi^-\pi^+\pi^-$ candidates with the fit results overlayed. The fit has several components: the $\Lambda_b^0 \to p\pi^-\pi^+\pi^-$ signal component is shown by the solid red line, combinatorial background is shown by the blue dashed line, partially reconstructed backgrounds from 5 body decays are shown by the light blue double dot dashed line, mis-identified $\Lambda_b^0 \to pK^-\pi^+\pi^-$ events are shown by the purple dot dash line and mis-identified $B^0 \to K^+\pi^-\pi^-\pi^+$ candidates are shown by the brown dashed line. The full fit is shown by the solid blue line. [6]

performed simultaneously to all four categories to extract the asymmetries $A_{\hat{T}}$ and $\bar{A}_{\hat{T}}$ (defined in Eqn (2)), from which the CP and P observables $a_{CP}^{\hat{T}-odd}$ and $a_p^{\hat{T}-odd}$ are calculated (defined in Eqn (3)).

Many resonances are expected in the four body $\Lambda_b^0 \to p\pi^-\pi^+\pi^-$ decay and it is expected different resonances will exhibit different levels of CP violation. It is entirely possible that the CP violation from different resonances would cancel if a phase space integrated asymmetry was calculated, which would considerably reduce the sensitivity of this search. Therefore, different regions of the phase space are investigated by calculating the $a_{CP}^{\hat{T}-odd}$ and $a_p^{\hat{T}-odd}$ observables for two separate binning schemes of the phase space. The first binning scheme, denoted "Scheme A", makes use of two body invariant masses in order to exploit the strong resonant structure from decays such as $\Delta(1232)^{++} \to p\pi^+$. "Scheme B" consists of 10 bins in the angle Φ which is the angle between the p π^-_{fast} and π^-_{slow} π^+ decay planes, shown in Figure 12. The objective of this binning scheme is to probe the interference between different resonant contributions.

Figure 13 shows the results for $a_{CP}^{\hat{T}-odd}$ and $a_p^{\hat{T}-odd}$ in each binning scheme. A χ^2 test is used to assess the compatibility of each binning scheme with the null hypothesis of CP symmetry; the p-values are $4.9 \times 10^{-2}(2.0\sigma)$ and $7.1 \times 10^{-4}(3.4\sigma)$ for the binning schemes A and B respectively. The combined significance of the measured level of CP violation in $\Lambda_b^0 \to p\pi^-\pi^+\pi^-$ decays is determined using a permutation test where 40,000 pseudoexperiments are generated with randomly assigned $\Lambda_b^0/\bar{\Lambda}_b^0$ flavour. The product of p-values from both binning schemes is compared between these pseudoexperiments and the values obtained in data, this leads to a combined significance for CP violation in $\Lambda_b^0 \to p\pi^-\pi^+\pi^-$ decays of 3.3σ. This is the first evidence for CP violation in a baryonic decay and it will be of great interest to study this asymmetry further when larger data samples are available.

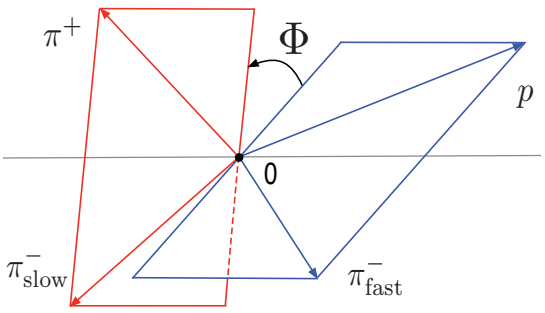

Figure 12. A diagram showing the defnition of the angle Φ which is used for binning scheme B. [6]

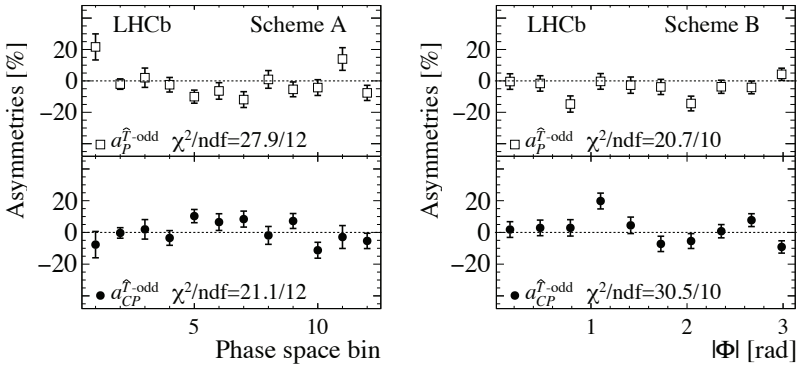

Figure 13. Left (Right): The CP(bottom) and P (top) violation asymmetries for binning scheme A(B). [6]

8 Summary

The study of charmless b hadron decays continues to yield many interesting results, and LHCb is leading the way in studying this sector. The branching fractions results for the $B^0_{(s)} \to K^0_S h^+ h'^-$ family of decays have been updated and the limits on the branching fraction of the $B^0_s \to K^0_S K^+ K^-$ have been narrowed. These results set the foundations for further Dalitz plot studies of these decay channels. Several baryonic decays of b mesons have been observed for the first time; the decay $B^0_s \to p\bar{\Lambda}K^-$ was the first baryonic decay of a B^0_s meson to be observed. The four body decays $B^0 \to p\bar{p}\pi^+\pi^-$, $B^0_s \to p\bar{p}K^+\pi^-$ and $B^0_s \to p\bar{p}K^+K^-$ have been observed for the first time, which open up opportunities for CP violation studies in four body baryonic b meson decays. A stringent upper limit has been set on the branching fraction of the decay $B^0_s \to \phi\eta'$, $\mathcal{B}(B^0_s \to \phi\eta') = 0.82(1.01) \times 10^{-6}$ at the 90%(95%) CL, which is a very useful input to the theoretical models used to predict the properties of $B^0_s \to PV$ decays. In the baryonic sector, the observation of the decay $\Xi^-_b \to pK^-K^-$ is the first observation of a charmless Ξ^-_b decay and opens up opportunities to search for CP violation in charmless Ξ^-_b decays. Lastly, 3.3σ evidence for CP violation in $\Lambda^0_b \to p\pi^-\pi^+\pi^-$ decays has been found; this is the first evidence for CP violation in a baryonic beauty decay. With further studies and larger data samples it is hoped these differences could contribute to understanding the absence of anti-matter in the universe.

References

[1] R. Aaij et al. (LHCb collaboration) (2017), submitted to JHEP, 1707.01665
[2] R. Aaij et al. (LHCb collaboration) (2017), submitted to Phys. Rev. D, 1704.08497
[3] R. Aaij et al. (LHCb collaboration), Phys. Rev. Lett. **119**, 041802 (2017), 1704.07908
[4] R. Aaij et al. (LHCb collaboration), JHEP **05**, 158 (2017), 1612.08110
[5] R. Aaij et al. (LHCb collaboration), Phys. Rev. Lett. **118**, 071801 (2017), 1612.02244
[6] R. Aaij et al. (LHCb collaboration), Nature Physics **13**, 391 (2017), 1609.05216
[7] R. Aaij et al., JINST **9**, P09007 (2014), 1405.7808
[8] M. Adinolfi et al., Eur. Phys. J. **C73**, 2431 (2013), 1211.6759
[9] M. Ciuchini, E. Franco, G. Martinelli, A. Masiero, L. Silvestrini, Phys. Rev. Lett. **79**, 978 (1997), hep-ph/9704274
[10] R. Aaij et al. (LHCb collaboration), Phys. Rev. Lett. **115**, 031601 (2015), 1503.07089
[11] R. Aaij et al. (LHCb collaboration), JHEP **10**, 143 (2013), 1307.7648
[12] R. Aaij et al. (LHCb collaboration), Int. J. Mod. Phys. **A30**, 1530022 (2015), 1412.6352
[13] T. Skwarnicki, Ph.D. thesis, Cracow, INP (1986), http://lss.fnal.gov/cgi-bin/find_paper.pl?other/thesis/skwarnicki.pdf
[14] H. Albrecht, H. Ehrlichmann, G. Harder, A. Krüger, A. Nau, A.W. Nilsson, A. Nippe, T. Oest, M. Reidenbach, M. Schäfer et al., Zeitschrift für Physik C Particles and Fields **48**, 543 (1990)
[15] G.J. Feldman, R.D. Cousins, Phys. Rev. **D57**, 3873 (1998), physics/9711021
[16] X. Fu, B. Nemati, S.J. Richichi, W.R. Ross, P. Skubic, M. Wood, M. Bishai, J. Fast, E. Gerndt, J.W. Hinson et al. (CLEO Collaboration), Phys. Rev. Lett. **79**, 3125 (1997)
[17] A.J. Bevan et al. (Belle, BaBar), Eur. Phys. J. **C74**, 3026 (2014), 1406.6311
[18] R. Aaij et al. (LHCb collaboration), Phys. Rev. Lett. **113**, 152003 (2014), 1408.0971
[19] E. Solovieva et al. (Belle), Phys. Lett. **B726**, 206 (2013), 1304.6931
[20] C.Q. Geng, Y.K. Hsiao, E. Rodrigues, Phys. Lett. **B767**, 205 (2017), 1612.08133
[21] R. Aaij et al. (LHCb collaboration), JHEP **09**, 006 (2015), 1505.03295
[22] C.Q. Geng, Y.K. Hsiao, Int. J. Mod. Phys. **A23**, 3290 (2008), 0801.0022
[23] C. Patrignani et al. (Particle Data Group), Chin. Phys. **C40**, 100001 (2016)
[24] M. Pivk, F.R. Le Diberder, Nucl.Instrum.Meth. **A555**, 356 (2005), physics/0402083
[25] C. Bebek, K. Berkelman, E. Blucher, J. Byrd, D.G. Cassel, E. Cheu, D.M. Coffman, T. Copie, G. Crawford, R. DeSalvo et al., Phys. Rev. Lett. **62**, 8 (1989)
[26] R. Aaij et al. (LHCb collaboration), Phys. Rev. Lett. **113**, 141801 (2014), 1407.5907
[27] C.Q. Geng, Y.K. Hsiao, J.N. Ng, Phys. Rev. Lett. **98**, 011801 (2007), hep-ph/0608328
[28] M. Beneke, M. Neubert, Nucl. Phys. **B675**, 333 (2003), hep-ph/0308039
[29] X.f. Chen, D.q. Guo, Z.j. Xiao (2007), hep-ph/0701146
[30] R. Aaij et al. (LHCb collaboration), Phys. Rev. Lett. **115**, 051801 (2015), 1503.07483
[31] K.S. Cranmer, Comput. Phys. Commun. **136**, 198 (2001), hep-ex/0011057
[32] W. Wang, Y.M. Wang, D.S. Yang, C.D. Lü, Phys. Rev. D **78**, 034011 (2008)
[33] H.Y. Cheng, C.W. Chiang, A.L. Kuo, Phys. Rev. D **91**, 014011 (2015)
[34] S.H. Zhou, Q.A. Zhang, W.R. Lyu, C.D. Lü, Eur. Phys. J. **C77**, 125 (2017), 1608.02819
[35] T. Aaltonen et al. (CDF), Phys. Rev. Lett. **103**, 031801 (2009), 0812.4271
[36] R. Aaij et al. (LHCb collaboration), JHEP **04**, 087 (2014), 1402.0770
[37] R. Aaij et al. (LHCb collaboration), JHEP **05**, 081 (2016), 1603.00413
[38] R. Aaij et al. (LHCb collaboration), Phys. Lett. **B759**, 282 (2016), 1603.02870

[39] R. Aaij et al. (LHCb collaboration), Phys. Rev. Lett. **110**, 221601 (2013), 1304.6173
[40] R. Aaij et al. (LHCb collaboration), Phys. Rev. **D90**, 112004 (2014), 1408.5373
[41] B. Aubert et al. (BaBar), Phys. Rev. Lett. **87**, 091801 (2001), hep-ex/0107013